TK 95 15
MKPH-T-95-07

DISPERSION–THEORETICAL ANALYSIS OF THE NUCLEON ELECTROMAGNETIC FORMFACTORS[#1]

P. Mergell[‡,*], Ulf-G. Meißner[†,⋆], D. Drechsel[‡,◇]

[‡]Universität Mainz, Institut für Kernphysik, J.-J.-Becher Weg 45
D–55099 Mainz, Germany

[†]Universität Bonn, Institut für Theoretische Kernphysik, Nussallee 14-16,
D–53115 Bonn, Germany

[*]electronic address: mergell@vkpmzp.kph.uni-mainz.de
[⋆]electronic address: meissner@pythia.itkp.uni-bonn.de
[◇]electronic address: drechsel@vkpmzp.kph.uni-mainz.de

Abstract

Dispersion relations allow for a coherent description of the nucleon electromagnetic form factors measured over a large range of momentum transfer, $Q^2 \simeq 0 \ldots 35$ GeV^2. Including constraints from unitarity and perturbative QCD, we present a novel parametrisation of the absorptive parts of the various isoscalar and isovector nucleon form factors. Using the current world data, we obtain results for the electromagnetic form factors, nucleon radii and meson couplings. We stress the importance of measurements at large momentum transfer to test the predictions of perturbative QCD.

[#1]Work supported in part by the Deutsche Forschungsgemeinschaft (SFB 201).

I. INTRODUCTION AND SUMMARY

The electromagnetic structure of the nucleon as revealed in elastic electron–nucleon scattering is parametrized in terms of the four form factors $F_{1,2}^{p,n}(Q^2)$ (with Q^2 the squared momentum transfer). The understanding of these form factors is of utmost importance in any theory or model of the strong interactions. Abundant data on these form factors over a large range of momentum transfer already exist, and this data base will considerably improve in the few GeV region when experiments at CEBAF will be completed and analysed. In addition, experiments involving polarized beams and/or targets are also performed at lower energies to give better data in particular for the electric form factor of the neutron, but also the magnetic proton and neutron ones. Such kind of experiments are under way at MAMI, ELSA, MIT-Bates and other places. Clearly, theory has to provide a tool to interpret these data in a model–independent fashion. Many years ago, dispersion theory was developed to extract these form factors from elastic ep and ed scattering data (and others) (for some early references, see e.g. [1] [2] [3].). Such a dispersion theoretical analysis is largely model–independent with the exception of the absorptive parts of the form factors, which are often parameterized in terms of a few meson poles. A large class of the early models of the spectral functions related to the imaginary parts of $F_{1,2}^{p,n}(Q^2)$ was based on the successful vector meson dominance (VMD) hypothesis (for reviews, see [4] [5]) which states that a photon couples to hadrons only via intermediate vector mesons. However, as already pointed out in 1959 by Frazer and Fulco [6] [7], such an approach is at odds with general constraints from unitarity. The two–pion continuum has a pronounced effect on the isovector spectral functions on the left wing of the ρ–resonance. This becomes particularly visible in the determinations of the corresponding nucleon radii. This effect was quantified by Höhler and Pietarinen [8] but has been neglected in most of the recent discussions of the nucleons form factors, like in [9] [10] [11] [12] [13]. For an accurate determination of the isovector nucleon radii, the inclusion of the two–pion cut contribution is mandatory. Another constraint comes from the accurate measurement of the neutron charge radius in very low-energy neutron–atom scattering (for a recent update, see e.g. Leeb and Teichmeister [14]). This leads to an additional normalization condition thus reducing the number of free parameters.[#2] Furthermore, in the framework of perturbative QCD (pQCD), the behaviour of the pertinent form factors for large momentum transfer can be inferred up to a model–dependent normalisation [16]. This has lead to models which try to synthezise aspects of low–energy hadron physics with the ones from pQCD, see e.g. [10] [11] [17] [18] [19] [20]. No clear picture has yet emerged at which momentum transfer the asymptotic behaviour really sets in. We stress here that any serious attempt to describe the electromagnetic structure of the nucleon has to account for *all* these constraints.

[#2] One can also consider the determination of the electric charge radius of the proton by Simon et al. [15] as a further low–energy constraint. It is, however, less stringent as the one related to the neutron charge radius and will be discussed separately in section II E.

The work presented here is an update and extension of the classical paper by Höhler and collaborators [21]. As in that paper, we determine the ρ–meson contribution to the isovector form factors from extended unitarity as discussed by Frazer and Fulco [7]. While we use the old πN partial waves extrapolated to the time–like regime [22], we update the pion form factor to account for the measured $\rho - \omega$ mixing [23]. In addition, since we are dealing with what is called an ill-posed problem, we restrict the number of additional pole terms in the isovector and isoscalar channel to a minimum (see the discussion below). We also implement the large–Q^2 behaviour dictated by pQCD, similar in spirit to the work of Furuichi and Watanabe [17] [18]. However, as we demonstrate later on, their choice of the spectral functions is not compatible with pQCD. What one ends up with is a set of superconvergence relations which reduce the number of free parameters. These superconvergence relations can be implemented in a variety of ways. Therefore, we will discuss two versions of the spectral functions with the proper asymptotic behaviour guided by simplicity and the notion of separating the hadronic from the pQCD contribution. A fit to the accessible data then allows not only to extract the nucleon electromagnetic form factors, but also the nucleon radii and nucleon–meson coupling constants. In particular, we also find a large coupling of the Φ–meson to the nucleon, seemingly in contradiction with the OZI–rule as stressed in the work by Genz and Höhler [24] and, more recently, by Jaffe [25]. It should be already noted here that this large Φ–nucleon coupling can be understood in terms of coupling of the photon to the kaon cloud surrounding the nucleon [26]. Our approach furthermore sheds light on the possible onset of pQCD and the regime where data are urgently called for. For a status review on the determination of the nucleon electromagnetic form factors, we refer to Höhler [27], Milner [28] and Bosted [29].

The pertinent results of this investigation can be summarized as follows:

(i) Including all the constraints discussed and using the current world data, we have found a new fit to the nucleon electromagnetic form factors. Besides the two–pion continuum and the pQCD contributions, we have three isoscalar and three isovector poles. This is the minimum number required by the data. We also stress that it is mandatory to *simultaneously* fit the proton and the neutron data.

(ii) The form factors $F_1^{(s)}(t)$ and $F_2^{(v)}(t)$ show a marked dipole structure. The reasons is that the two lowest poles in the respective channels are not too far separated in mass and appear with residua of the same magnitude but different in sign. In the isoscalar case, this is due to the closeness of the ω and Φ mesons [21]. The novel feature of our study is that the first pole above the two–pion continuum can be identified with the $\rho'(1450)$ leading to the dipole structure in $F_2^{(v)}(t)$. We furthermore find the third isoscalar and the second isovector pole at $M_{S'} = 1.60$ GeV and $M_{\rho''} = 1.65$ GeV. Only the third isovector pole cannot be identified with a physical state.

(iii) We have given a new determination of the electric and magnetic radii of the proton and the neutron. We find $r_E^p = 0.847$ fm, $r_M^p = 0.853$ fm and $r_M^n = 0.889$ fm, all with an uncertainty of about 1%. These are consistent with the findings of ref. [21] with the exception of the neutron magnetic radius. The difference is mainly due to the neglect of the superconvergence relation related to the asymptotic behaviour of $F_2^{(v)}$ in [21].

(iv) We have shown that the accurate determination of the proton charge radius in ref. [15] is only consistent with the dispersive analysis within one standard deviation. Using the central value of ref. [15] for r_E^p, one can*not simultaneously* fit the proton and the neutron data.

(v) We have determined the vector (g_1) and tensor (g_2) couplings of the ω and the Φ mesons. The g_1 are slightly larger than in Ref. [21] while the g_2 are of comparable size. We stress again that the large ΦNN coupling does not indicate a violation of the OZI–rule but rather accounts for the neglect of the $\bar{K}K$ continuum.

(vi) In our best fit, the parameter Λ^2, which is a measure of the boundary between the hadronic (pole) and quark (pQCD) contributions, comes out to be $\Lambda^2 \simeq 10$ GeV^2. Only in the case of the proton magnetic form factor one has data at suffciently large momentum transfer to possibly test the predictions of pQCD. Our conclusion is that even in that case more data are needed to really see the asymptotic behaviour $Q^4 G_M^p(Q^2) \to$ constant (modulo logarithms). For all form factors there is still a sizeable hadronic contribution in the momentum transfer range between $Q^2 = 10 \ldots 20$ GeV^2. In particular, the data available for the ratio $Q^2 F_2(Q^2)/F_1(Q^2)$ are at too low momentum transfer to indicate any scaling.

(vii) The fits are completely insensitive to the number of flavors entering via the anomalous dimension appearing in the asymptotic behaviour of the form factors and to the $\rho - \omega$ mixing which comes in via the calculation of the isovector two–pion unitarity correction.

(viii) More accurate data at *low*, *intermediate* and (very) *large* momentum transfer are called for to further tighten the constraints on the radii and coupling constants and to really test the pQCD predictions.

The manuscript is organized as follows. In section II we discuss the basic concepts underlying the dispersion–theoretical analysis of the nucleon electromagnetic form factors. In particular, we summarize the various constraints which have to be implemented to obtain a consistent picture. These are the inclusion of the two–pion continuum in the isovector spectral functions (sect. II C), the determination of the neutron charge radius from very low energy neutron–atom scattering (sect. II D) and the behaviour of the various form factors as given by pQCD (sect. II F). We also discuss another less stringent constraint related to the proton charge radius (sect. II E). Section III contains the form factor parametrizations we will use. We present two forms, one in which the pQCD constraints are implemented in the most simple fashion and another one, which allows for a separation between the hadronic (pole) and the pQCD terms already on the level of the spectral functions. The results are presented and discussed in section IV. The appendices A and B contain some technicalities, and in appendix C, we give the explicit parametrization of our best fit.

II. BASIC CONCEPTS

In this section, we assemble all tools necessary for the construction of the fit functions for the spectral distributions discussed in section III. We also supply the basic definitions and notations underlying our analysis. In particular, we discuss the various low and high energy constraints which have to be imposed and allow to reduce the number of free parameters. This material is mostly not new but necessary to keep the manuscript self–contained. The reader familiar with it is invited to skip this section.

A. Definition of the nucleon electromagnetic form factors

The matrix–element of the electromagnetic (em) current $\mathcal{J}_\mu$ sandwiched between nucleon states can be expressed in terms of two form factors,

$$< N(p') \,|\, \mathcal{J}_\mu \,|\, N(p) >= e\, \bar{u}(p') \Big\{ \gamma_\mu \, F_1(t) + \frac{i}{2m_N} \, \sigma_{\mu\nu} \, Q^\nu \;\; F_2(t) \Big\} \, u(p) \;\; , \tag{1}$$

with m_N the nucleon mass, $t = (p' - p)^2 = -Q^2$ the invariant momentum transfer squared and $t < 0$ in the space–like region. $F_1(t)$ and $F_2(t)$ are called the Dirac and the Pauli form factor, respectively. They are normalised at $t = 0$ as

$$F_1^p(0) = 1 \, , \quad F_1^n(0) = 0 \, , \quad F_2^p(0) = \kappa_p \, , \quad F_2^n(0) = \kappa_n \; , \tag{2}$$

with κ_p (κ_n) the anomalous magnetic moment of the proton (neutron) in units of the nuclear magneton, $\mu_N = e/2m_N$. For later use, we also need the isospin decomposition, i.e. the response of the nucleon to the isoscalar (denoted by the superscript '(s)') and isovector (denoted by the superscript '(v)') components of the electromagnetic current,

$$F_i^{(s)} = \frac{1}{2}(F_i^p + F_i^n) \, , \quad F_i^{(v)} = \frac{1}{2}(F_i^p - F_i^n) \, , \quad (i = 1, 2) \, , \tag{3}$$

with the normalisation

$$F_i^I(0) = \nu_i^I \;\; , \quad i = 1, 2 \, ; \quad I = (v), (s) \; , \tag{4}$$

where

$$\nu_1^{(s)} = \nu_1^{(v)} = \frac{1}{2} \; , \; \nu_2^{(s)} = \frac{1}{2}(\kappa_p + \kappa_n) \; , \; \nu_2^{(v)} = \frac{1}{2}(\kappa_p - \kappa_n) \; . \tag{5}$$

One can also introduce the so–called Sachs form factors $G_{E,M}^{p,n}(Q^2)$ related to the $F_1(Q^2)$ and $F_2(Q^2)$ via

$$G_E(Q^2) = F_1(Q^2) - \tau F_2(Q^2) \, , \quad G_M(Q^2) = F_1(Q^2) + F_2(Q^2) \, , \quad \tau = \frac{Q^2}{4m_N} \, . \tag{6}$$

In the Breit frame, G_E and G_M are nothing but the Fourier–transforms of the charge and the magnetization distribution, respectively.

The slope of the form factors at $t = 0$ is conventionally expressed in terms of a nucleon radius $< r^2 >^{1/2}$,

$$F(t) = F(0) \left(1 + \frac{1}{6} < r^2 > \, t + \ldots \right) \tag{7}$$

which is rooted in the non–relativistic description of the scattering process, in which a point-like charged particle interacts with a given charge distribution $\rho(r)$. The mean square radius of this charge distribution is given by

$$< r^2 > = \int_0^\infty dr \, 4\pi r^2 \rho(r) = -\frac{6}{F(0)} \frac{dF(Q^2)}{dQ^2}\Big|_{Q^2=0} \, . \tag{8}$$

Eq.(8) can be used for all form factors except G_E^n and F_1^n which vanish at $t = 0$. In these cases, one simply drops the normalization factor $1/F(0)$ and defines e.g. the neutron charge radius via

$$< r^2 >_n^{\rm ch} = -6 \, \frac{dG_E^n(Q^2)}{dQ^2}\Big|_{Q^2=0} \, . \tag{9}$$

To conclude this section, we remark that the slopes of G_E^n and F_1^n are related via

$$\frac{dG_E^n(Q^2)}{dQ^2}\Big|_{Q^2=0} = \frac{dF_1^n(Q^2)}{dQ^2}\Big|_{Q^2=0} - \frac{F_2^n(0)}{4m_N^2} \, . \tag{10}$$

The second term in eq.(10) is called the Foldy term. It gives the dominant contribution to the slope of G_E^n.

B. Dispersion relations for the nucleon em form factors

Let $F(t)$ be a generic symbol for any one of the four nucleon em form factors $F_{1,2}^{(v,s)}(t)$. We assume the validity of an unsubtracted dispersion relation of the form[#3]

$$F(t) = \frac{1}{\pi} \int_{t_0}^\infty \frac{{\rm Im}\, F(t')}{t' - t} \, dt' \, . \tag{11}$$

The spectral function Im $F(t)$ is different from zero along the cut from t_0 to ∞ with $t_0 = 4\,(9)\,M_\pi^2$ for the isoscalar (isovector) case and M_π denotes the pion mass. The proof of the validity of such dispersion relations in QCD has not yet been given [30]. Eq.(11) means that the em structure of the nucleon is entirely determined from its absorptive behaviour.

[#3]Since the normalization $F(0)$ is known, one could also work with once–subtracted dispersion relation.

Data for $F(t)$ are given for $t < 0$. If these would be infinitively precise, the continuation to other values of $t > 4M_\pi^2$ would be unique. However, the available data have certain error bars which make the continuation unstable as detailed in the review [31]. This is what one calls an ill–posed problem. Therefore, one needs some additional assumptions which should have a physics motivation. We follow here the prescription due to Sabba–Stefanescu [32] and require that the spectral functions should not have more than the minimum number of oscillations and parameters required by the data. To make this more specific, let us consider as an example the rather successful dipole fit,

$$G_E^P(t) \simeq \mu_p G_M^p(t) \simeq \mu_n G_M^n(t) \simeq G_D(t)\,, \quad G_D(t) = (1 - t/0.71\,\mathrm{GeV}^2)^{-2}\,, \tag{12}$$

where μ_p and μ_n are the magnetic moments of the proton and the neutron, respectively. Such a form is only possible if the corresponding spectral functions contain at least two pole terms with opposite signs.

Of particular interest is the VMD approach in which the spectral functions are approximated by a few vector meson poles, namely the $\rho, \ldots$ in the isovector and the $\omega, \Phi, \ldots$ in the isoscalar channel, in order. In that case, the form factors take the form

$$F_i^{(I)}(t) = \sum_V \frac{a_i^{(I)}}{M_{(I)}^2 - t} \quad i = 1,2\,; \quad I = v, s\,, \tag{13}$$

with

$$a_i^V = \frac{M_V^2}{f_V}\, g_i^{VNN}\,, \quad V = \rho, \omega, \Phi, \ldots\,, i = 1,2\,. \tag{14}$$

In many fits, the mass parameters M_V are taken from the known meson masses and the strength parameters a_i^V are fitted. This in turn leads to a determination of the various vector–meson–nucleon coupling constants, g_i^{VNN}. Note, however, that such a procedure becomes increasingly arbitrary for higher mass excitations. One defines the ratio of the tensor to vector coupling, κ_V, via

$$\kappa_V = \frac{g_2^{VNN}}{g_1^{VNN}}\,. \tag{15}$$

One expects e.g. κ_ρ to be large (~ 6) and κ_ω to be small (~ 0). In strict VMD, one has $\kappa_\rho = \kappa_p - \kappa_n = 3.71$ and $\kappa_\omega = \kappa_p + \kappa_n = -0.12$. The coupling constants f_V are known from the widths of the leptonic decays $V \to e^+e^-$, i.e.

$$\frac{f_V^2}{4\pi} = \frac{\alpha^2}{3}\frac{M_V}{\Gamma(V \to e^+e^-)}\,. \tag{16}$$

Clearly, such pole terms contribute to the spectral functions in terms of δ–functions,

$$\mathrm{Im}F_i^V(t) = \pi\, a_i^V\, \delta(t - M_V^2)\,. \tag{17}$$

Of course, there are other contributions related to intermediate states like $n\pi$ ($n \geq 2$), $N\bar{N}$, $K\bar{K}$ and so on. As we will discuss in section II C, of these the 2π intermediate states play the most important role.

C. Constraints from unitarity

Here, we briefly summarize what is known about the contribution of the two–pion continuum to the isovector spectral functions and how this should be implemented. The unitarity relation of Frazer and Fulco [7] determines the isovector spectral functions from $t = 4M_\pi^2$ to $t \simeq 50 M_\pi^2 \simeq 1$ GeV^2 in terms of the pion form factor $F_\pi(t)$ and the P–wave $\pi\pi N\bar{N}$ partial wave amplitudes, cf. Fig.1. We use here the form

$$\mathrm{Im}F_i^{(v),2\pi}(t) = \frac{q_t^3}{\sqrt{t}}\,|F_\pi(t)|^2\,J_i(t)\,, \quad i = 1,2 \tag{18}$$

with $q_t = \sqrt{t/4 - M_\pi^2}$ and the functions $J_i(t)$ are related to the P–wave πN partial waves in the t–channel, $f_\pm^1(t)$, via

$$f_\pm^1(t) = F_\pi(t)\,J_\pm(t)\;, \tag{19}$$

in the conventional isospin decomposition. The $J_i(t)$ are tabulated in [33]. For the pion form factor, we use the recent parametrization of Barkow et al. [23] which takes into account $\rho-\omega$ mixing,

$$F_\pi(t) = F_\pi^\rho(t)\frac{1+\alpha_\omega F_\pi^\omega(t)}{1+\alpha_\omega} \tag{20}$$

with α_ω the mixing parameter, $\alpha_\omega = 0.0038$ [23]. The functions $F_\pi^V(t)$ $(V = \rho,\omega)$ are of the standard Gounaris–Sakurai form [34]. A typical result for the corresponding isovector spectral functions (weighted with $1/t^2$) is shown in Fig.2. One notices the strong enhancement close to two–pion threshold. The reason for this behaviour has been known for long. The partial waves $f_\pm^1(t)$ have a branch point singularity on the second sheet (from the projection of the nucleon pole terms) located at

$$t_c = 4M_\pi^2 - M_\pi^4/m_N^2 = 3.98\,M_\pi^2\;, \tag{21}$$

very close to the physical threshold at $t_0 = 4M_\pi^2$. The isovector form factors inherit this singularity and the closeness to the physical threshold leads to the pronounced enhancement. Note that in the VMD approach this spectral function is given by a δ–function peak at $M_\rho^2 \simeq 30 M_\pi^2$ and thus the isovector radii are strongly underestimated if one neglects the unitarity correction [8] as can be seen from the formula

$$< r^2 >_i^{(v),2\pi} = \frac{6}{\pi}\int_{4M_\pi^2}^{50M_\pi^2}\frac{dt'}{t'^2}\,\mathrm{Im}F_i^{(v),2\pi}(t')\;. \tag{22}$$

Consequently, in the isovector channels one should not use a simple ρ pole but rather work with the spectral functions as given by eq.(18). This is the procedure adopted here. To speed up the numerical calculations, one can fit the corresponding two–pion contributions to the isovector form factors via (as it was done in [21])

$$F_i^{(v),2\pi}(t) = F_i^\rho(t) = \frac{a_i^\rho + b_i^\rho (1 - t/c_i^\rho)^{-2/i}}{2\,(1 - t/d_i^\rho)}\,, \quad i = 1,2 \tag{23}$$

with $a_1^\rho = 1.0317$, $a_2^\rho = 5.7824$, $b_1^\rho = 0.0875$, $b_2^\rho = 0.3907$, $c_1^\rho = 0.3176$, $c_2^\rho = 0.1422$, $d_1^\rho = 0.5496$ and $d_2^\rho = 0.5362$. We have also performed fits with the exact representation eq.(18) which lead to the same results as the use of the form eq.(23). To end this section, we remark that the form eq.(18) is exact below four–pion threshold, $t = 16M_\pi^2$ and we stop at $t_{\rm up} = 50M_\pi^2$ since the pion form factor shows some structure on the right wing of the ρ–peak which can not simply be fitted by a superposition of Gounaris–Sakurai functions. In the isoscalar channel, it is believed that the pertinent spectral functions rise smoothly from the three–pion threshold to the ω peak, i.e. that there is no pronounced effect from the three–pion cut on the left wing of the ω–resonance (which also has a much smaller width than the ρ). Chiral perturbation theory [35] [36] or an investigation of the spectral functions related to the process $N\bar{N} \to 3\pi$ could be used to settle this issue. The one loop calculation of the isovector nucleon form factors indeed shows the unitarity correction on the left wing of the ρ [35]. For the isoscalar form factors, a two loop calculation of the pertinent imaginary parts would reveal whether there is some enhancement around $t = 9M_\pi^2$ or justify the common assumption that one has a smooth isoscalar spectral functions driven by the ω at low t.

D. Constraints from low–energy neutron–atom scattering

There exists a large number of experiments trying to determine the neutron–electron scattering length b_{ne} from low–energy neutron–atom scattering. The interest in this quantity stems from its direct relation to the mean square radius of the neutron,

$$b_{ne} = \frac{\alpha m_n}{3} < r^2 >_n^{\rm ch}\,, \tag{24}$$

or

$$\left.\frac{dG_E^n(Q^2)}{dQ^2}\right|_{Q^2=0} = -14.39\,[\text{fm}]\, b_{ne}\,, \tag{25}$$

with $\alpha = e^2/4\pi = 1/137.036$ the fine structure constant. For an early review, see e.g. Foldy [37]. There has been some controversy about the actual value of b_{ne} over the years as discussed in [14]. We use here the most recent value, $b_{ne} = (-1.308 \pm 0.05) \cdot 10^{-3}$ fm [38] which leads to (adding systematic and statistical errors in quadrature)

$$-6\left.\frac{dF_1^n(Q^2)}{dQ^2}\right|_{Q^2=0} = (0.0136 \pm 0.0043)\,\text{fm}^2\,, \tag{26}$$

using eq.(10). Notice that due to the large cancellation between the Foldy term and the slope of G_E^n, the slope of F_1^n is very sensitive to the value of b_{ne}. If one uses e.g. the older value of Koester et al. [39], $b_{ne} = (-1.32 \pm 0.04) \cdot 10^{-3}$ fm, one finds $-6dF_1^n/dQ^2 = (0.0126 \pm 0.0035)$ fm^2. The slope of $F_1^n(Q^2)$ as given in eq.(26) will be imposed on all our fits.

E. Constraints from low–energy electron–proton scattering

Simon et al. [15] have presented a precise measurement and analysis of their and other existing data for elastic electron–proton scattering in the range $Q^2 = 0.005 \ldots 0.055$ GeV^2. They have performed a fit of the type

$$G_E^p(Q^2) = a_0 \Big(1 + Q^2 \frac{a_1}{a_0} + Q^4 \frac{a_2}{a_0} \Big) \ , \tag{27}$$

with adjustable parameters a_0, a_1, a_2. The proton charge radius is thus given by

$$\frac{1}{G_E^p(0)} \frac{dG_E^p(Q^2)}{dQ^2}\Big|_{Q^2=0} = \frac{a_1}{a_0} = -\frac{< r_E^2 >_p}{6a_0} \ . \tag{28}$$

For the data in the low–energy region, the contribution of the Q^4 term to the proton electric form factor is marginal ($< 0.3\%$). This leads to an rather accurate value for $< r_E^2 >_p$,

$$< r_E^2 >_p = (0.862 \pm 0.012) \text{ fm}^2 \ . \tag{29}$$

With that constraint, the authors of [15] performed a four pole fit (with two masses fixed at $M_\rho = 0.765$ GeV and $M_{\rho'} = 1.31$ GeV) to the available data for the proton electric and magnetic form factors up to $Q^2 \simeq 5$ GeV^2. This allowed to reconstruct the spectral function $\text{Im}G_E^v(t)$. It is in agreement with the one of ref. [8] with the exception of the region around $t = 7M_\pi^2$. One could now argue that the dispersive analysis to be performed should be constrained by the value of the proton radius, eq.(29). In that case one would, of course, have to exclude the low–energy data ($Q^2 < 0.6$ GeV^2) from the data basis. So as not to exclude the possibility of new and more precise data also for G_E^p at low Q^2, we will perform a set of fits with all data included and another set with the constraint eq.(29) imposed and the corresponding data removed. We consider this as a good measure of the accuracy in determining the various nucleon radii from a dispersion–theoretical analysis.

F. Constraints from perturbative QCD

Perturbative QCD allows to constrain the behaviour of the nucleon em form factors for large momentum transfer, $Q^2 = -t \to \infty$. In its most simple fashion, the so–called quark counting rules [40] give the leading power in the large–Q^2 fall–off of the form factors by counting the number of gluon exchanges which are necessary to distribute the large photon momentum equally to all constituents. In the limit $-t \to \infty$ this leads to

$$(-t)^{i+1} F_i(t) \to \text{constant} \ , \quad i = 1, 2 \tag{30}$$

which in turn translates into a set of superconvergence relations for the spectral functions,

$$\frac{1}{\pi} \int_{t_0}^{\infty} dt' \, \text{Im}F_1(t') = 0 \ , \tag{31}$$

$$\frac{1}{\pi}\int_{t_0}^{\infty} dt'\,\mathrm{Im}F_2(t') = \frac{1}{\pi}\int_{t_0}^{\infty} dt'\,t'\,\mathrm{Im}F_2(t') = 0\ , \tag{32}$$

for both the proton and the neutron. These arguments have been sharpened in [16]. There, it was shown that the magnetic Sachs form factor takes the form

$$G_M(Q^2) = \ C\,\frac{\alpha_s^2(Q^2)}{Q^4}\Big[\ln\Big(\frac{Q^2}{Q_0^2}\Big)\Big]^{\frac{2}{3\beta}}\ , \tag{33}$$

with $\alpha_s(Q^2)$ the running strong coupling constant,

$$\alpha_s(Q^2) = \frac{4\pi}{\beta\,\ln(Q^2/Q_0^2)}\,, \quad \beta = 11 - \frac{2}{3}N_f\ . \tag{34}$$

Here, N_f is the number of flavors, β the QCD β–function to one loop and $Q_0 \simeq \Lambda_{\rm QCD}$. The constant C in eq.(33) is model–dependent and subject of much controversy. Its explicit form is not needed here. Taking furthermore into account that any helicity–flip leads to an extra $1/Q$ factor, one finds

$$F_i(t) \to (-t)^{-(i+1)}\left[\ln\Big(\frac{-t}{Q_0^2}\Big)\right]^{-\gamma}, \quad \gamma = 2 + \frac{4}{3\beta}\ , \quad i = 1,2\ . \tag{35}$$

The anomalous dimension γ depends weakly on the number of flavors, $\gamma = 2.148,\ 2.160,\ 2.173$ for $N_f = 3,\ 4,\ 5$, in order. In what follows, we will construct spectral functions which lead exactly to the large–t behaviour as given in eq.(35).

III. PARAMETRIZATION OF THE FORM FACTORS

We have now assembled all tools to construct parametrizations of the nucleon form factors subject to the constraints discussed in the previous section. We will present two such parametrizations. The first one, which we label 'multiplicative', is guided by simplicity. For the second one, called 'additive', the spectral function is split in a way which allows for a clearer separation between the hadronic (pole) and the pQCD contributions.

A. Multiplicative parametrization

Consider the functions

$$F_i^{(s)}(t) = \tilde{F}_i^{(s)}(t)L(t) = \Big[\sum_s \frac{a_I^{(s)}\,L^{-1}(M_{(s)}^2)}{M_{(s)}^2 - t}\Big]\left[\ln\Big(\frac{\Lambda^2 - t}{Q_0^2}\Big)\right]^{-\gamma}\ , \tag{36}$$

$$F_i^{(v)}(t) = \tilde{F}_i^{(v)}(t)L(t) = \Big[\tilde{F}_i^{\rho}(t) + \sum_v \frac{a_I^{(v)}\,L^{-1}(M_{(v)}^2)}{M_{(v)}^2 - t}\Big]\left[\ln\Big(\frac{\Lambda^2 - t}{Q_0^2}\Big)\right]^{-\gamma}\ , \tag{37}$$

$$L(t) \equiv \left[\ln\Big(\frac{\Lambda^2 - t}{Q_0^2}\Big)\right]^{-\gamma} \ , \tag{38}$$

where the parameter Λ can be considered as a measure of the onset of the asymptotic behaviour. The value of Q_0 is strongly correlated to the one of Λ in the actual fits, we choose its value to be in the few hundred MeV region (as discussed in section IV), $Q_0 \sim \Lambda_{\rm QCD}$. We take into account three poles in the isovector (v) channels and denote these by ρ', ρ'' and ρ'''.[#4] The ρ contribution is fixed by extended unitarity as discussed in section II C,

$$\tilde{F}_i^\rho(t) = \frac{1}{\pi}\int_{4M_\pi^2}^{50M_\pi^2} dt' \, \frac{{\rm Im}F_i^\rho(t')}{L(t')(t'-t)} = \frac{a_i^\rho L^{-1}(M_a^2) + b_i^\rho L^{-1}(M_b^2)(1-t/c_i^\rho)^{-2/i}}{2(1-t/d_i^\rho)} \ , \tag{39}$$

with the mass parameters M_a and M_b determined from a fit to $\tilde{F}_i^\rho(t)$ and the $a_i^\rho, b_i^\rho, c_i^\rho, d_i^\rho$ given after eq.(23). We find $M_a^2 = 0.5$ GeV^2 and $M_b^2 = 0.4$ GeV^2. In the isoscalar channels, we have three meson poles, the first two with fixed masses at $M_\omega = 0.782$ GeV and $M_\Phi = 1.02$ GeV plus one heavier state denoted by S'. The contribution of $L(t)$ for momenta smaller than Λ is balanced by the appropriate normalization factors at the meson poles, $L^{-1}(M_I^2)$, $I = (v), (s)$.

The analytic structure of the functions $F_i^I(t)$ in the complex t-plane is shown in Figs.3a,b. In the isovector case (Fig.3b), $I = (v)$, the two–pion continuum leads to a cut from $t_0 = 4M_\pi^2$ to $t_{\rm up} = 50M_\pi^2$. In addition, there are poles at $t = M_{\rho'}, M_{\rho''}, M_{\rho'''}$ which to some extent compensate the neglect of cuts related to higher mass continua like 4π, $N\bar{N}$ and so on (with positive G–parity). At larger values of t along the real axis, there is a singularity at $t_{\rm sing} = \Lambda^2 - Q_0^2$ from the logarithm plus a cut from $t_{\rm sing}$ to Λ^2 since the exponent γ appearing in $L(t)$, eq.(38), is rational. Finally, there is the right–hand cut from Λ^2 to ∞. The only difference in the isoscalar case (Fig.3a), $I = (s)$, is that one has three poles at M_ω^2, M_Φ^2 and $M_{S'}^2$. The latter two simulate cuts related to multi–pion and other intermediate states with negative G–parity. The singularity at $t_{\rm sing}$ has no physical significance, it is related to the way in which the large—t behaviour is enforced. We will come back to this point in the next subsection.

The normalization conditions of the form factors at $t = 0$ take the form

$$\rho_i^{(-1)}\,\delta_{I,(v)} + \sum_I a_i^I \, \frac{L^{-1}(M_I^2)}{M_I^2} = \nu_i^I \, L^{-1}(0) \tag{40}$$

with the ν_i^I given in eq.(5) and [17]

$$\rho_i^{(k)} = \frac{1}{\pi}\int_{4M_\pi^2}^{50M_\pi^2} dt' \, t'^k \, {\rm Im}F_i^\rho(t') L^{-1}(t') = \frac{1}{2}\Big(a_i^\rho \, L^{-1}(M_a^2)\,(d_i^\rho)^{k+1} + b_i^\rho \, L^{-1}(M_b^2)\,\delta_{k,-1}\Big) \ . \tag{41}$$

[#4] This notation, however, should not imply a priori that these poles have to be identified with higher mass excitations of the ρ. This topic will be taken up again when we discuss the actual results of our fits.

The conditions on the neutron charge radius, eq.(26), and on the proton charge radius, eq.(29), translate into

$$\frac{dF_1^I}{dt}(0)\,L(0) = \sum_I \frac{a_1^I L^{-1}(M_I^2)}{M_I^2}\Big(\frac{1}{M_I^2} + \frac{\gamma}{\Lambda^2 L^{-1/\gamma}(0)}\Big)$$

$$+\delta_{I,(v)}\Big[\Big(a_1^\rho L^{-1}(M_a^2) + b_1^\rho L^{-1}(M_b^2)\Big)\Big(\frac{1}{d_1^\rho} + \frac{\gamma}{2\Lambda^2 L^{-1/\gamma}(0)}\Big) + 2\frac{b_1^\rho L^{-1}(M_b^2)}{c_1^\rho}\Big]\ ,\quad I = (v),(s)\,. \tag{42}$$

If one only imposes the value of the neutron charge radius, one has to take the appropriate linear combination of the two conditions given in eq.(42). We stress again that this latter case should be considered as more realistic. The implementation of the pQCD constraints, eq.(35), via the logarithmic function $L(t)$ is similar to the approach taken in [10,11,26]. The following superconvergence relations have to be fulfilled so that the proper pQCD asymptotics emerges [17]

$$\rho_i^{(0)}\,\delta_{I,(v)} + \sum_I a_i^I\, L^{-1}(M_I^2) = 0\ ,$$
$$\rho_2^{(1)}\,\delta_{I,(v)} + \sum_I M_I^2\, a_2^I\, L^{-1}(M_I^2) = 0\ . \tag{43}$$

These relations assure that the pole-terms and the 2π–continuum do only contribute to subleading orders as $|t|$ becomes large. In Appendix A, we discuss how all these constraints are technically implemented.

Finally, let us count the number of free parameters for the fit functions eqs.(36,37). For $n_s = 3$ isoscalar and $n_v = 3$ isovector mesons, one gets $2(n_s+n_v) = 12$ pole and $(n_s+n_v) = 6$ mass parameters plus the pQCD parameter Λ. We remark here that we do not treat Q_0 as a free parameter since only the combination $L^{-1}(0) = [\ln(\Lambda^2/Q_0^2)]^\gamma$ enters the pertinent formulae. We only make sure that Q_0 comes out in the few hundred MeV region because of its proportionality to $\Lambda_{\rm QCD}$. We also stress that the ρ contribution does not induce any free parameter and that the mass of the lowest two isoscalar poles are fixed to M_ω and M_ϕ. With the 12 relations eqs.(40,42,43) the effective number of free parameters is thus $18 + 1 - 2 - 12 = 5$ (or 6 if we only enforce the condition on the neutron charge radius).

B. Additive parametrization

The form factor representation eqs.(36,37) is very simple but one can not directly separate the hadronic from the pQCD contribution in the spectral functions. Therefore, we present here another form which is similar in spirit to the one proposed in ref. [17]. Under some approximations, one can in fact construct a spectral representation for the pQCD part which can be added to the contributions from the meson poles and the two-pion continuum. This in

general introduces some additional fit parameters c_i^I which are related to the normalization of the form factors at large t,

$$F_i^I(t) \to \frac{c_i^I}{t^{i+1}\,[\ln(-t/Q_0^2)]^\gamma}\ . \tag{44}$$

In addition, one has to take special care about the singularity at $t_{\rm sing}$ as detailed in appendix B. It leads to an extra pole term not considered in [17] [18]. The explicit additive parametrization takes the form

$$\begin{aligned}
{\rm Re}F_i^I(t) &= \frac{\delta_{I,(v)}}{\pi}\int_{4M_\pi^2}^{50M_\pi^2} dt' \frac{{\rm Im}F_i^\rho(t')}{t'-t} + \sum_I \frac{a_i^I}{M_I^2-t} + c_i^I \bar{F}_i^{I,{\rm QCD}} \\
\bar{F}_i^{I,{\rm QCD}} &= \frac{\tilde{a}_i^{\rm QCD}}{\Lambda^2-Q_0^2-t} + \frac{1}{\pi}\int_{\Lambda^2}^\infty dt' \frac{{\rm Im}\bar{F}_i^{\rm QCD}(t')}{t'-t}\ , \\
{\rm Im}\bar{F}_i^{\rm QCD}(t) &= \frac{\sin\Big(\gamma\Big[\arctan(\frac{\pi}{\ln(z)}) + \pi\Theta(1-z)\Big]\Big)}{\Big((\ln(z))^2+\pi^2\Big)^{\gamma/2}\ t^{i+1}}\ ,
\end{aligned} \tag{45}$$

with $z = |(\Lambda^2 - t)/Q_0^2|$. Clearly, the representation for the Im $F_i^{\rm QCD}$ is more complicated than the one used in [17] [18] but it leads to the desired behaviour, eq.(44). The normalization and radius constraints as well as the superconvergence relations are modified,

$$\begin{aligned}
\rho_i^{(-1)}\,\delta_{I,(v)} + \sum_I \frac{a_i^I}{M_I^2} + \frac{a_i^{I,{\rm QCD}}}{\Lambda^2-Q_0^2} + c_i^I\,\xi_i^{(-1)} &= \nu_i^I \\
\rho_i^{(0)}\,\delta_{I,(v)} + \sum_I a_i^I + a_i^{I,{\rm QCD}} + c_i^I\,\xi_i^{(0)} &= 0\ , \\
\rho_2^{(1)}\,\delta_{I,(v)} + \sum_I M_I^2\,a_2^I + (\Lambda^2-Q_0^2)\,a_2^{I,{\rm QCD}} + c_2^I\,\xi_2^{(1)} &= 0\ , \\
\frac{a_1^{I,{\rm QCD}}}{(\Lambda^2-Q_0^2)^2} + c_1^I\,\xi_1^{(-2)} + \sum_I \frac{a_1^I}{M_I^4} + \delta_{I,(v)}\,\rho_1^{(-2)} &= \frac{dF_1^I}{dt}(0)\ ,
\end{aligned} \tag{46}$$

with

$$\xi_i^{(k)} = \frac{1}{\pi}\int_{\Lambda^2}^\infty dt'\,t'^k\,{\rm Im}F_i^{\rm QCD}(t')\ . \tag{47}$$

Here, the $\rho_i^{(k)}$ are defined as in eq.(41) with $L(t) \equiv 1$, and the $a_i^{I,{\rm QCD}}$ are defined in appendix B. The pertinent numerical values are $dF_1^{(s)}(0)/dt = 1.37\,{\rm GeV}^{-2}$ and $dF_1^{(v)}(0)/dt = 1.30\,{\rm GeV}^{-2}$. These last two conditions in eq.(46) have to be combined appropriately if only the neutron charge radius as measured in low–energy neutron–atom scattering is enforced (i.e. only one constraint results). In the additive parametrization, eq.(45), we have in principle three[#5] more effective free parameters than in the multiplicative one. In the latter

[#5] Since we take the value of Λ^2 as given from the multiplicative parametrization, only three of the c_i^I are independent.

case, the normalization of the form factors at large momentum transfer are essentially fixed by our choice of the functions $L(t)$. We stress here that the values one obtains for the parameters c_i^I are only indicative of the strength of the form factors in the asymptotic region since their numerical values are very sensitive to the number of meson poles at low energies one accounts for (see also [17] [18]). In fact, what can happen in the additive parametrization is the following. If one does not give reasonable bounds on the new parameters c_i^I, a simple χ^2–minimization can lead to unphysical results with very large $|c_i^I|$. These will then influence the low–t behaviour of the various form factors, in particular the isoscalar radii. Therefore, we constrain the additive parametrization to essentially give the same low momentum description of the four em form factors as does the multiplicative one. This also means that the c_i^I are fixed, i.e. they are no longer free parameters (see also app.B). This method ensures that we can make sensible statements about the pQCD contributions to the various spectral functions. Only if one would have data at larger Q^2 it would make sense leaving the c_i^I as free parameters.

C. Fits with an effective ρ pole

The inclusion of the ρ contribution as detailed in section II C leads to a large value for the tensor–vector coupling ratio (as defined in eq.(15)) [22],

$$\kappa_\rho = 6.6 \pm 1 \ . \tag{48}$$

This value is in agreement with other determinations, see e.g. Grein [41] ($\kappa_\rho = 6.1 \pm 0.6$). More recently, Brown and Machleidt [42] have discussed the evidence for a strong ρNN coupling from the measurements of the ϵ_1 parameter in NN scattering. In ref. [17] an effective ρ pole with a mass of 0.63 GeV was used and led to typical values of $\kappa_\rho = 5.9$. We will also perform such a simple pole fit, i.e. substituting the full two–pion continuum by a ρ pole with a variable mass and taking in addition two more pole terms in the isovector channels. Our motivation to perform such types of simplified fits is to check whether the large value of the tensor–to–vector coupling of the ρ with the correct implementation of the pQCD constraints can be considered a generic result.

IV. RESULTS AND DISCUSSION

Before discussing the specific results of our fits, we wish to make some general comments. We had argued before that the masses of the three isovector excitations and of the highest isoscalar one need not to coincide with masses of physical particles. However, we have found that it is possible to find a minimum in the χ^2 hyper–surface fixing $M_{\rho'} = 1.45$ GeV and $M_{\rho''} = 1.69$ GeV together with $M_{S'} = 1.60$ GeV. These are the values of the most recent particle data group compilation [43] for the lowest isovector–vector and isoscalar–vector meson excitations. Leaving the values of these masses completely free does not alter the

χ^2 significantly. In contrast, the mass of the third pole in the isovector channel is tightly bound due to the various constraints the fits have to obey. We observe that the mass of this third isovector pole tends to come out close to one of the other isovector poles, thus an effective double–pole structure around $M_{\rho'}$ or $M_{\rho''}$ emerges. This is in marked contrast to the findings of ref. [21]. However, it is mandatory to retain three poles besides the two–pion cut contribution in the isovector channel. Also, independent of the details of the fits, we find that while the form factors $F_1^{(s)}(t)$ and $F_2^{(v)}(t)$ exhibit a stable dipole structure (i.e. the lowest two poles have residua which are equal in magntiude but with different signs), this is not the case for $F_2^{(s)}(t)$ and $F_1^{(v)}(t)$. These findings agree with the ones of [21]. Concerning the accuracy of our fits, all normalization, radius and superconvergence relations are fulfilled within machine accuracy, typically much better than one part in 10^{12}. After these general remarks, we turn to a more detailed description of our results.

A. The best fit: Form factors, radii and coupling constants

The optimal fit to the available set of form factor data is obtained with the isovector masses of 1.45, 1.65 and 1.69 GeV, respectively and the isoscalar ones being 0.782, 1.019 and 1.60 GeV. The corresponding residua are $a_1^{\rho'} = -3.465$, $a_2^{\rho'} = -6.552$, $a_1^{\rho''} = 40.26$, $a_2^{\rho''} = 7.881$, $a_1^{\rho'''} = -37.30$, $a_2^{\rho'''} = -2.821$, $a_1^{\omega} = 0.747$, $a_2^{\omega} = -0.122$, $a_1^{\Phi} = -0.738$, $a_2^{\Phi} = 0.162$, $a_1^{S'} = -0.0382$ and $a_2^{S'} = -0.0406$. We find $\Lambda^2 = 9.73$ GeV^2 and $Q_0^2 = 0.35$ GeV^2. We notice that to have good fits, we can vary Λ^2 between 5 and 15 GeV^2 without drastically changing any of our conclusions. We always work with $\gamma = 2.148$ since the fits are completely insensitive to the possible variation in this quantity. In this fit, only the constraint on the neutron charge radius is imposed and the $\rho - \omega$ mixing in the two–pion spectral function is included. The resulting χ^2/datum is 1.09.

In Fig.4, we show the electric and magnetic proton and neutron form factors normalised to the dipole fit.[#6] Similar to earlier findings, we note that there are substantial deviations from the dipole fit in all channels, particularly at large momentum transfer. We also note that a better data basis is clearly needed.

Of particular importance is the determination of the nucleon radii. In table 1, we give radii corrsponding to the Pauli and Dirac form factors in comparison to the results of ref. [21]. For the isovector form factors, the radii are indeed dominated by the two–pion plus ρ contribution, we have $r_1^\rho \simeq r_2^\rho \simeq 0.75$ fm. The corresponding neutron and proton radii are given in table 2. The uncertainty for these radii is 1% (for comparison, in [21] the uncertainties on the radii were of the order of 3%). This number is calculated in the following way. In the parameter–space we look for solutions with a comparable χ^2/datum than the best fit has. Equivalently, one can sum in quadrature the 1σ deviations of these

---

[#6] In the case of G_E^n, we divide by G_E^n as given by Platchkov et al. [44] (denoted by G_P) since in the dipole approximation, $G_E^n \equiv 0$.

parameters contributing to the various radii. Our results are comparable to the ones of ref. [21] with the exception of $r_2^{(v)}$ and r_M^n. This can be traced back to the fact that in [21] the superconvergence relation

$$\frac{1}{2} a_2^\rho (d_2^\rho)^2 + \sum_{V=\rho',\rho'',\rho'''} a_2^V \, M_V^2 = 0 \ , \tag{49}$$

was not taken into account. In contrast, our values for $r_2^{(v)}$ and r_M^n are based on a completely consistent calculation. We point out that there exist some on–going activity e.g. at ELSA (Bonn) to determine the neutron magnetic form factor more precisely at low and moderate momentum transfer. We also note that the value for r_E^p is on the low side of the result of ref. [15]. If one insists on their central value, $r_E^p = 0.862$ fm, by imposing the proper slope condition, one is not able to simultaneously fit the neutron and the proton form factor data. In fact, in [15] only proton data were considered. We conclude that the uncertainty attributed to r_E^p in [15] is presumably underestimated. As we already anticipated in section II E, the constraint from the proton charge radius in its present form is too restrictive to be applied in the dispersive analysis. Better low–energy data are clearly called for to settle this issue.

The mesonic coupling constants can be directly inferred from the pertinent residua. Applying the same analysis to get a handle at the uncertainties as described above, we find

$$\begin{aligned} g_1^{\omega NN} &= 20.86 \pm 0.25 \ , \quad g_2^{\omega NN} = -3.41 \pm 0.24 \ , \\ g_1^{\Phi NN} &= -9.16 \pm 0.23 \ , \quad g_2^{\Phi NN} = 2.01 \pm 0.33 \ , \end{aligned} \tag{50}$$

which are compared with the findings of ref. [21] in table 3. Our Φ–couplings are somewhat larger but consistent within error bars. We note that the ωNN coupling is larger than in typical one–boson exchange potentials or from the analysis of Grein and Kroll [45] using forward dispersion relations for NN–scattering, $(g_1^{\omega NN})^2/4\pi = 8.1 \pm 1.5$. Such a small coupling constant value cannot be accomodated in our fit, it is inconsistent with empirical information on the slope of $F_1^{(s)}$ if the ω and the Φ lead to the dipole structure as described above. This point is also discussed in some detail in [27]. Furthermore, we remark that a direct comparison with coupling constants obtained in boson–exchange models, which in general include strong meson-nucleon form factors, has to be taken cum grano salis.[#7]. In flavor SU(3), one can derive the following formulae for the $\omega - \Phi$–mixing angle, Θ,

$$\frac{\sqrt{3}}{\cos(\Theta)} \frac{g_1^{\rho NN}}{g_1^{\omega NN}} - \tan(\Theta) = \frac{g_1^{\Phi NN}}{g_1^{\omega NN}} \ . \tag{51}$$

[#7] The photon couplings through vector mesons to the nucleon need not be the same than the purely strong interaction VNN couplings

Using $g_1^{\rho NN} = 2.6$ [22], we have $\Theta = 35°$, very close to the ideal mixing angle of 37°. This means that the Φ is almost entirely an $\bar{s}s$ state and is thus supposed to decouple from the nucleon (to leading order in flavor perturbation theory). This is the much discussed violation of the OZI rule. This apparent paradox finds its resolution in the fact that the simple pole approach for the ΦNN coupling effectively includes contributions from the $\bar{K}K$ continuum. Stated differently, the Φ can couple to the kaon cloud surrounding the nucleon (as modeled e.g. in [26]). This topic could be investigated further along the lines discussed in section II C, i.e. by analyzing the $\bar{N}N \to \bar{K}K$ partial waves.

We close the discussion about the coupling constants with some remarks on κ_ρ. As argued in section III C, one can also perform fits with a ρ–pole. In this case, one cannot take the physical mass for the ρ since otherwise the isovector radii are severely underestimated. We have performed such fits and find

$$\kappa_\rho = 6.1 \pm 0.2 \ , \tag{52}$$

which is consistent with previous determinations as discussed in section III C. We consider this an important consistency check on our fits. The realistic fits, however, have to include the correlated two–pion exchange as described in section II C.

Next, we discuss the large momentum behaviour of the form factors. Only for G_M^p, there are data for $Q^2 > 10$ GeV^2. In Fig.5, we show the quantities $Q^4 G_M^p(Q^2)/\mu_p$ and $L^{-1}(Q^2) Q^4 G_M^p(Q^2)/(\mu_p L^{-1}(0))$ up to $Q^2 = 50$ GeV^2. Within the uncertainties, the curve representing the second function tends to a constant (as it is expected from pQCD), but it is obvious that more precise data at high momentum transfer are mandatory to really pin down this behaviour. The available data do not exclude that asymptotia sets in much beyond $Q^2 = 30$ GeV^2. Often considered is also the ratio $Q^2 F_2(Q^2)/F_1(Q^2)$ which should become constant as Q^2 becomes large (the extra Q^2 in front of F_2 compensates the spin–flip suppression $\sim 1/Q^2$). In this ratio, many uncertainties related to the exact form of the nucleon wave function drop out. As seen in Fig.6, the presently available data are at too low momentum transfer to test this prediction, although there is some hint of $Q^2 F_2(Q^2)/F_1(Q^2)$ becoming constant as Q^2 increases. Again, more accurate data at higher Q^2 are called for.

B. Additive parametrization: Hadron versus quark contributions

As explained before, the multiplicative parametrization is not well suited for separating the hadronic (pole) from the quark (pQCD) contributions. That is the reason underlying the additive parametrization. In this case, the four normalization constants c_i^I (of which only three are independent) in principle increase the number of tuneable parameters. However, as explained before, one has to impose certain constraints on the actual values of the c_i^I since otherwise completely unphysical solutions of the fitting procedure can emerge. Our strategy is therefore to constrain pole parameters and the c_i^I such that we essentially recover the low momentum description of the multiplicative parametrization, in particular the nucleon

radii. Only with such constraints one can make sensible statements about the separation of hadronic and pQCD contributions.

In Fig.7, we show a typical result for the isoscalar and isovector form factors. We have $c_1^{(v)} = -53.40$, $c_1^{(s)} = -8.20$, $c_2^{(v)} = 95.56$ and $c_2^{(s)} = -1.55$. The χ^2/datum is 1.86. This increased value is a mostly reflection of the the approximations performed (i.e. the neglect of subleading $1/t$ corrections) to derive the additive parametrization, compare app.B.[#8] We repeat that leaving all parameters free, one could naturally find a solution with a lower χ^2 than for the multiplicative parametrizations. Such solutions, however, have to be discarded as discusssed before. For all form factors, the hadronic and the quark contribution are of comparable size (in magnitude) around $\Lambda^2 \simeq 10$ GeV^2. We notice that for the Dirac form factors $F_1^{(s,v)}(Q^2)$, the hadronic contribution quickly drops off beyond Q^2 larger than 10 GeV^2. For the Pauli form factors $F_2^{(s,v)}(Q^2)$, this fall–off is slower which essentially is the reason that one does not observe pQCD scaling for the available data. In all cases, the quark contribution is very small at low t (by construction). A similar behaviour was noticed in [17], [18] although in these papers the asymptotic behaviour was incorrectly implemented in the spectral functions. Of course, with the presently available data base, these results should only be considered indicative. With better data in the few and many GeV region, one will eventually be able to more cleanly separate the hadronic from the quark contribution. In particular, for the range of momentum transfer available at CEBAF, one will essentially probe the transition region from the hadronic to the quark description. The planned experiments at CEBAF [46] will certainly shed light on this interesting regime.

ACKNOWLEDGEMENTS

We thank Gerhard Höhler for many informative discussions and Ralf Gothe for providing us with the most recent ELSA data. We are also grateful to Wulf Krümpelmann for supplying us with his data basis.

[#8] In that appendix, it is also shown how one can systematically improve this procedure. For our purpose, the lowest order approximation used here is, however, sufficient.

APPENDIX A: IMPLEMENTATION OF THE CONSTRAINTS

In this appendix we show how to evaluate the fit constraints. In general we have a system of 12 equations. It can be written in the following way,

$$\hat{M}_i^I \vec{A}_i^I = \vec{C}_i^I \quad , \tag{A1}$$

where the matrix $\hat{M}_i^I$ has the form

$$\hat{M}_i^I = \begin{pmatrix} M_{I_1}^{-2} & M_{I_2}^{-2} & M_{I_3}^{-2} \\ 1 & 1 & 1 \\ \tilde{M}_{I_1} & \tilde{M}_{I_2} & \tilde{M}_{I_3} \end{pmatrix} \quad , \quad \tilde{M}_I = \sigma \cdot \begin{cases} \frac{1}{M_I^4} + \kappa \frac{\gamma L^{1/\gamma}(0)}{M_I^2 \Lambda^2} & , \quad i = 1 \\ M_I^2 & , \quad i = 2 \end{cases} . \tag{A2}$$

Setting $\sigma = 1,\ 0$, respectively, permits to switch off certain vector meson pole terms. κ specifies the parametrization. $\kappa = 1$ if the multiplicative parametrization is used and $\kappa = 0$ for the additive one. With $A_i^I = a_i^I L^{-1}(M_I^2)$ we can write

$$\vec{A}_i^I = \begin{pmatrix} A_i^{I_1} \\ A_i^{I_2} \\ A_i^{I_3} \end{pmatrix} \quad , \quad \vec{C}_i^I = \begin{pmatrix} \nu_i^I L^{-1}(0) - \rho_i^{(-1)} \delta_{I,(v)} \\ -\rho_i^{(0)} \delta_{I,(v)} \\ \tilde{C}_i^I \end{pmatrix} \quad . \tag{A3}$$

The vector $\vec{C}_i^I$ contains all fit constraints. The first component enforces the correct normalizations, the second and the last one in the case $(i = 2)$ induce the superconvergence relation (43). For $(i = 1)$ the third component implies the slope informations stemming from the experimental values of the electric radii of proton and neutron,

$$\tilde{C}_i^I = \begin{cases} \frac{dF_1^I}{dt}(0) L^{-1}(0) - \Re \delta_{I,(v)} & , \quad i = 1 \\ -\rho_2^{(1)} \delta_{I,(v)} & , \quad i = 2 \end{cases} , \tag{A4}$$

where $\Re$ is the contribution of the two pion continuum to the radius constraints

$$\Re = \left(a_1^\rho L^{-1}(M_a^2) + b_1^\rho L^{-1}(M_b^2) \right) \left(\frac{1}{d_1^\rho} + \kappa \frac{\gamma L^{1/\gamma}(0)}{2\Lambda^2} \right) + 2 \frac{b_1^\rho L^{-1}(M_b^2)}{c_1^\rho} \quad . \tag{A5}$$

We simply invert the matrix $\hat{M}_i^I$ to find the solution vector $\vec{A}_i^I$,

$$(\hat{M}_i^I)^{-1} = \frac{1}{m} \begin{pmatrix} \tilde{M}_{I_3} - \tilde{M}_{I_2} & M_{I_3}^{-2} \tilde{M}_{I_2} - M_{I_2}^{-2} \tilde{M}_{I_3} & M_{I_2}^{-2} - M_{I_3}^{-2} \\ \tilde{M}_{I_1} - \tilde{M}_{I_3} & M_{I_1}^{-2} \tilde{M}_{I_3} - M_{I_3}^{-2} \tilde{M}_{I_1} & M_{I_3}^{-2} - M_{I_1}^{-2} \\ \tilde{M}_{I_2} - \tilde{M}_{I_1} & M_{I_2}^{-2} \tilde{M}_{I_1} - M_{I_1}^{-2} \tilde{M}_{I_2} & M_{I_1}^{-2} - M_{I_2}^{-2} \end{pmatrix} \quad , \tag{A6}$$

with

$$m = (M_{I_2}^{-2} - M_{I_3}^{-2}) \tilde{M}_{I_1} + (M_{I_3}^{-2} - M_{I_1}^{-2}) \tilde{M}_{I_2} + (M_{I_1}^{-2} - M_{I_2}^{-2}) \tilde{M}_{I_3} \quad . \tag{A7}$$

APPENDIX B: DERIVATION OF THE ADDITIVE PARAMETRIZATION

Here, we derive the additive parametrization, eq.(45). The Cauchy integral representation for the fit functions $F_i^I(t)$ $(i = 1, 2; I = (v), (s))$, eqs.(36,37), takes the form

$$F_i^I(t) = \frac{1}{2\pi i} \oint_{\mathcal{C}_I} dt' \frac{F_i^I(t')}{t' - t} \ , \tag{B1}$$

with $\mathcal{C}_I$ a closed integration contour as shown in Figs.3a,b. $\mathcal{C}_I$ is chosen such that Re $F_i^I(t)$ can be calculated as a Hilbert-transform. For that, we need the imaginary part of $F_i^I(t)$,

$$\text{Im } F_i^I(t \pm i\epsilon) = \text{Re } \tilde{F}_i^I(t) \, \text{Im } L(t \pm i\epsilon) + \text{Im } \tilde{F}_i^I(t \pm i\epsilon) \, \text{Re } L(t) \ . \tag{B2}$$

The real and imaginary parts of $F_i^I(t)$ for $t < t_{\text{sing}} = \Lambda^2 - Q_0^2$ and $t > t_{\text{sing}}$ can be deduced easily. $L(t)$ is purely real for $t < t_{\text{sing}}$. Consider now the imaginary part of $L(t)$. For $t_{\text{sing}} < t < \Lambda^2$, we find (on the first Riemann sheet)

$$\text{Im } L(t \pm i\epsilon) = \mp \frac{\sin(\gamma\pi)}{|\ln(z)|^\gamma} \ , \tag{B3}$$

with

$$z = \left| \frac{\Lambda^2 - t}{Q_0^2} \right| \ , \tag{B4}$$

and for $t > \Lambda^2$, it reads (on the first sheet)

$$\text{Im } L(t \pm i\epsilon) = \mp \frac{\sin\Big(\gamma \Big[\arctan(\frac{\pi}{\ln(z)}) + \pi\Theta(1-z) \Big] \Big)}{\Big((\ln(z))^2 + \pi^2 \Big)^{\gamma/2}} \ , \tag{B5}$$

and finally

$$\text{Im } L(\Lambda^2 \pm i\epsilon) = 0 \ , \tag{B6}$$

assuming that $M_I^2 < \Lambda^2$ for all I. Due to the singularity at t_{sing}, special care has to be taken of the region $t \in [\Lambda^2 - 2Q_0^2, \Lambda^2]$. We have

$$\text{Re } F_i^I(t) = \frac{1}{\pi} \int_{\Lambda^2}^\infty dt' \frac{\text{Re } \tilde{F}_i^I(t') \, \text{Im } L(t)}{t' - t} + \frac{1}{2\pi} \text{Im} \left[\oint_{\mathcal{C}_I^{\text{sing}}} dt' \frac{F_i^I(t')}{t' - t} \right] + \dots \ , \tag{B7}$$

where the ellipsis stands for the contributions from the pole terms and the two–pion continuum (which are of no relevance for the large–t behaviour discussed here). For the contour

$\mathcal{C}_I^{\rm sing}$ we choose a closed circle around the singularity with radius Q_0^2. In the region of integration and close to the singularity, we have $t \gg M_I^2$ so that we can approximate $\tilde{F}_i^I(t)$ by its asymptotic behaviour [#9].

$$\mathrm{Re}\; F_i^I(t) = \frac{c_i^I}{\pi}\int_{\Lambda^2} dt' \frac{\mathrm{Im}\; L(t)}{(t')^{i+1}\,(t'-t)} + \frac{c_i^I}{2\pi}\mathrm{Im}\left[\oint_{\mathcal{C}_I^{\rm sing}} dt' \frac{L(t')}{(t')^{i+1}\,(t'-t)}\right] + \dots \ . \tag{B8}$$

Let us concentrate on the second term in eq.(B8). Parametrizing the integration path via $t(\phi) = t_{\rm sing} + Q_0^2 \exp(i\phi)$, we find

$$I(t) = \frac{1}{2\pi}\int_0^{2\pi} d\phi \frac{iQ_0^2 e^{i\phi}\ln(1-e^{i\phi})^{-\gamma}}{[\Lambda^2 - Q_0^2(1-e^{i\phi})]^{i+1}[\Lambda^2 - t - Q_0^2(1-e^{i\phi})]} \ . \tag{B9}$$

We expand the first term in the numerator in eq.(B9),

$$\frac{1}{[\Lambda^2 - Q_0^2(1-e^{i\phi})]^{i+1}} = \frac{1}{[\Lambda^2 - Q_0^2]^{i+1}}\left(1 - (i+1)\frac{Q_0^2}{\Lambda^2 - Q_0^2}\, e^{i\phi} + \dots\right) , \tag{B10}$$

and drop the term proprotional to $\exp(i\phi)$ in the numerator of eq.(B9). Altogether, we find

$$I(t) = i\,\frac{\tilde{a}_I^{\rm QCD}}{\Lambda^2 - Q_0^2 - t} \ , \tag{B11}$$

with

$$\tilde{a}_I^{\rm QCD} = \frac{Q_0^2}{2\pi(\Lambda^2 - Q_0^2)^{i+1}}\left[C^{(1)} - (i+1)\frac{Q_0^2}{\Lambda^2 - Q_0^2}\, C^{(2)} + \dots\right] ,$$
$$C^{(n)} = \int_0^{2\pi} d\phi\, e^{in\phi}\ \ln(1-e^{i\phi})^{-\gamma} \qquad , \tag{B12}$$

where the coefficients $C^{(n)}$ can be found by numerical integration. They are purely real. It is sufficient to keep the first two terms in the series with $C^{(1)} = -5.861$ and $C^{(2)} = 7.129$. Setting now

$$a_i^{I,{\rm QCD}} = c_i^I\ \tilde{a}_i^{\rm QCD} \ , \tag{B13}$$

we have arrived at the desired result, eq.(45).

Finally, we wish to establish a more rigorous derivation which is useful if one wants to retain more terms of the asymptotic expansion of the $F_i^I(t)$. For that, we expand the $\tilde{F}_i^I(t)$ in powers of $1/t$,

$$\tilde{F}_i^I(t) = \sum_{k_i \le (i+1)}^{\infty} c_{k_i}^I\, t^{-k_i} \ , \tag{B14}$$

[#9] In our fits, the most massive isovector (isoscalar) pole is at 2.8 (2.6) GeV^2, which is a bit close to the value of $\Lambda^2 \simeq 10$ GeV^2. This induces some uncertainty due to the terms neglected.

with the coefficients $c^I_{k_i}$ given by

$$c^I_{k_i} = (-)^{k_i}\left(\sum_I a^I_i\, M_I^{2\,(k_i-1)}\, L^{-1}(M_I^2) + \frac{\delta_{I,(v)}}{\pi}\int_{4\,M_\pi^2}^{50\,M_\pi^2} dt'(t')^{k_i-1}\mathrm{Im}\,F_i^\rho(t')L^{-1}(t')\right)\ , \quad \text{(B15)}$$

and

$$c^I_{k_i<(i+1)} = 0 \quad \text{(B16)}$$

because of the superconvergence relations. This leads to

$$\mathrm{Re}\ F_i^I(t) = \sum_{k_i\le(i+1)}^{\infty} c_{k_i}\left(\frac{1}{\pi}\int_{\Lambda^2}^{\infty} dt'\frac{\mathrm{Im}\ L(t)}{(t')^{k_i}\,(t'-t)} + \frac{1}{2\pi}\mathrm{Im}\left[\oint_{\mathcal{C}_I^{\mathrm{sing}}} dt'\frac{L(t')}{(t')^{k_i}\,(t'-t)}\right]\right) + \dots\ , \quad \text{(B17)}$$

which can be written in a form similar to eq.(45)

$$\mathrm{Re}F_i^I(t) = \frac{a_i^{I,\mathrm{QCD}}}{\Lambda^2 - Q_0^2 - t} + \frac{1}{\pi}\int_{\Lambda^2}^{\infty} dt'\frac{\mathrm{Im}F_i^{\mathrm{QCD}}(t')}{t'-t}\ + \dots\ , \quad \text{(B18)}$$

but in this case we find

$$a_i^{I,\mathrm{QCD}} = \sum_{k_i\le(i+1)}^{\infty}\frac{c^I_{k_i}\,Q_0^2}{2\pi(\Lambda^2-Q_0^2)^{k_i}}\left[C^{(1)} - k_i\frac{Q_0^2}{\Lambda^2-Q_0^2}\,C^{(2)} + \dots\right]\ ,$$

$$\mathrm{Im}F_i^{\mathrm{QCD}}(t) = \mathrm{Re}\tilde{F}_i^I(t)\,\mathrm{Im}L(t)\ . \quad \text{(B19)}$$

Considering only the first term of the sum over k_i in eq.(B19) is equivalent to the approximation eq.(B8).

APPENDIX C: PARAMETRIZATION OF THE BEST FIT

Here we give the parametrization of the best fit discussed in section IV A explicitly for easy usage, with Q^2 in GeV^2,

$$F_1^{(s)}(Q^2) = \left[\frac{9.464}{0.611+Q^2} - \frac{9.054}{1.039+Q^2} - \frac{0.410}{2.560+Q^2}\right]\left[\ln\left(\frac{9.733+Q^2}{0.350}\right)\right]^{-2.148}\ ,$$

$$F_2^{(s)}(Q^2) = \left[-\frac{1.549}{0.611+Q^2} + \frac{1.985}{1.039+Q^2} - \frac{0.436}{2.560+Q^2}\right]\left[\ln\left(\frac{9.733+Q^2}{0.350}\right)\right]^{-2.148}\ ,$$

$$F_1^{(v)}(Q^2) = \left[\frac{1.032\left[\ln\left(\frac{9.733-0.500}{0.350}\right)\right]^{2.148} + 0.088\left[\ln\left(\frac{9.733-0.400}{0.35}\right)\right]^{2.148}\left(1+\frac{Q^2}{0.318}\right)^{-2}}{2\left(1+\frac{Q^2}{0.550}\right)} - \right.$$
$$\left.\frac{38.885}{2.103+Q^2} + \frac{425.007}{2.734+Q^2} - \frac{389.742}{2.835+Q^2}\right]\left[\ln\left(\frac{9.733+Q^2}{0.350}\right)\right]^{-2.148}\ ,$$

$$F_2^{(v)}(Q^2) = \left[\frac{5.782\left[\ln\left(\frac{9.733-0.500}{0.350}\right)\right]^{2.148} + 0.391\left[\ln\left(\frac{9.733-0.400}{0.350}\right)\right]^{2.148}\left(1+\frac{Q^2}{0.142}\right)^{-1}}{2\left(1+\frac{Q^2}{0.536}\right)} - \right.$$
$$\left.\frac{73.535}{2.103+Q^2} + \frac{83.211}{2.734+Q^2} - \frac{29.467}{2.835+Q^2}\right]\left[\ln\left(\frac{9.733+Q^2}{0.350}\right)\right]^{-2.148}\ . \quad \text{(C1)}$$

Tables

	$r_1^{(s)}$ [fm]	$r_2^{(s)}$ [fm]	$r_1^{(v)}$ [fm]	$r_2^{(v)}$ [fm]
Best Fit	0.782	0.845	0.765	0.893
Ref. [21]	0.77	0.837	0.76	0.863

Table 1: Radii of the Dirac and Pauli form factors.

	r_E^p [fm]	r_M^p [fm]	r_M^n [fm]	r_1^p [fm]	r_2^p [fm]	r_2^n [fm]
Best Fit	0.847	0.836	0.889	0.774	0.894	0.893
Ref. [21]	0.836	0.843	0.840	0.761	0.883	0.876

Table 2: Proton and neutron radii.

	$(g_1^{\omega NN})^2/4\pi$	κ_ω	$(g_1^{\Phi NN})^2/4\pi$	κ_Φ
Best Fit	34.6 ± 0.8	-0.16 ± 0.01	6.7 ± 0.3	-0.22 ± 0.01
Ref. [21]	30 ± 3	-0.17	4.4 ± 1	-0.3

Table 3: Coupling constants of the isoscalar vector mesons.

REFERENCES

[1] G.F. Chew et al., Phys. Rev.110 (1958) 265
[2] P. Federbush, M.L. Goldberger and S.B. Treiman, Phys. Rev. 112 (1958) 642
[3] S.D. Drell and F. Zachariasen, "Electromagnetic Structure of Nucleons", Oxford University Press, Oxford, 1960
[4] S. Blatnik and N. Zovko, Acta Physica Austriaca 39 (1974) 62
[5] J.J. Sakurai, "Currents and Mesons", The University of Chicago Press, Chicago, 1969
[6] W.R. Frazer and J.R. Fulco, Phys. Rev. Lett. 2 (1959) 365
[7] W.R. Frazer and J.R. Fulco, Phys. Rev. 117 (1960) 1603, 1609
[8] G. Höhler and E. Pietarinen , Phys. Lett. B53 (1975) 471
[9] J.G. Körner and M. Kuroda, Phys. Rev. D16 (1977) 2165
[10] M.F. Gari and W. Krümpelmann, Z. Phys. A322 (1985) 689
[11] M.F. Gari and W. Krümpelmann, Phys. Lett. B173 (1986) 10
[12] S. Dubnicka, Nuovo Cimento 100A (1988) 1
[13] S. Dubnicka, Nuovo Cimento 103A (1990) 1417
[14] H. Leeb and C. Teichmeister, Phys. Rev. C48 (1993) 1719
[15] G.G. Simon et al., Nucl. Phys. A333 (1980) 381
[16] S.J. Brodsky and P.G. Lepage, Phys. Rev. D22 (1980) 2157
[17] S. Furuichi and K. Watanabe, Prog. Theor. Phys. 82 (1989) 581
[18] S. Furuichi and K. Watanabe, Prog. Theor. Phys. 83 (1990) 567
[19] R. Jakob, P. Kroll, M. Schürmann and W. Schweiger, Z. Phys. A338 (1991) 339
[20] P. Kroll, M. Schürmann and W. Schweiger, Z. Phys. A347 (1993) 109
[21] G. Höhler et al., Nucl. Phys. B114 (1976) 505
[22] G. Höhler and E. Pietarinen, Nucl. Phys. B95 (1975) 210
[23] L.M. Barkov et al., Nucl. Phys. B256 (1985) 365
[24] H. Genz and G. Höhler, Phys. Lett. B61 (1976) 389
[25] R.L. Jaffe, Phys. Lett. B229 (1989) 275
[26] M.F. Gari and W. Krümpelmann, Phys. Lett. B274 (1992) 159
[27] G. Höhler, πN Newsletter 9 (1993) 108; "Analysis of Nucleon electromagnetic Formfactors", University of Karlsruhe preprint, 1995 (in preparation)
[28] R.G. Milner, "Nucleon Form Factors", MIT preprint No. 94/71, Fifth Conf. on the Intersections of Particle and Nuclear Physics, 1994
[29] P.E. Bosted, Phys. Rev. C51 (1995) 409
[30] R. Oehme, πN Newsletter 7 (1992) 1
[31] S. Ciulli, C. Pomponiu, I. Sabba–Stefanescu, Phys. Reports 17 (1975) 133
[32] I. Sabba–Stefanescu, J. Math. Phys. 21 (1980) 175
[33] G. Höhler, "Pion-Nucleon Scattering", Landolt–Börnstein Vol.I/9b, ed. H. Schopper, Springer, Berlin, 1983
[34] G.J. Gounaris and J.J. Sakurai, Phys. Rev. Lett. 21 (1968) 244
[35] J. Gasser, M.E. Sainio and A. Švarc, Nucl. Phys. B307 (1988) 779
[36] V. Bernard, N. Kaiser and Ulf-G. Meißner, Bonn University preprint TK 95 1, 1995, Int. J. Mod. Phys. E, in print
[37] L.L. Foldy, Rev. Mod. Phys. 30 (1958) 471
[38] S. Kopecky, P. Riehs, J.A. Harvey and N.W. Hill, Phys. Rev. Lett. 74 (1995) 2427
[39] L. Koester, W. Waschkowski and J. Meier, Z. Phys. A329 (1988) 229
[40] S.J. Brodsky and G. Farrar, Phys. Rev. D11 (1975) 1309
[41] W. Grein, Nucl. Phys. B131 (1977) 255
[42] G.E. Brown and R. Machleidt, Phys. Rev. C50 (1994) 1731
[43] Particle Data Group, M. Aguilar–Benitez et al., Phys. Rev. D50 (1994) 1173
[44] S. Platchkov et al., Nucl. Phys. A510 (1990) 740
[45] W. Grein and P. Kroll, Nucl. Phys. B137 (1978)173; Nucl. Phys. A338 (1980) 332; Nucl. Phys. A377 (1982) 505
[46] CEBAF proposals PR93-038, PR93-026, PR91-010, PR91-017

[47] W. Albrecht et al., Phys. Lett. B26 (1968) 642
[48] S. Rock et al., Phys. Rev. Lett. 49 (1982) 1139
[49] A. Lung et al., Phys. Rev. Lett. 70 (1993) 718
[50] S. Galster et al., Nucl. Phys. B32 (1971) 221
[51] C.E. Woodward et al., Phys. Rev. C44 (1991) R571
[52] T. Eden et al., Phys. Rev. C50 (1994) R1749
[53] M. Meyerhoff et al., Phys. Lett. B327 (1994) 201
[54] C.H. Berger et al., Phys. Lett. B35 (1971) 87
[55] W. Bartel et al., Phys. Lett. B33 (1970) 245
[56] W. Albrecht et al., Phys. Rev. Lett. 17 (1966) 1192
[57] T. Jansens et al., Phys. Rev. 142 (1965) 922
[58] F Borkowski et al., Nucl. Phys. B93 (1975) 461
[59] G.G. Simon et al., Z. Naturforschung 35a (1980) 1
[60] R.C. Walker, thesis California Institute of Technology, 1989, unpublished
[61] P.E. Bosted et al., Phys. Rev. Lett. 68 (1992) 3841
[62] P.N. Kirk et al., Phys. Rev. D8 (1973) 63
[63] P. Stein et al., Phys. Rev. Lett. 16 (1966) 592
[64] E.B. Hughes et al., Phys. Rev. 141 (1965) 458
[65] C.W. Akerlof et al., Phys. Rev. B135 (1964) 810
[66] J.R. Dunning et al., Phys. Rev. 141 (1966) 1357
[67] B. Schoch, Prog. Part. Nucl. Phys. 34 (1995) 43;
R. Gothe, private communication
[68] R. Arnold et al., Phys. Rev. Lett. 57 (1986) 174
[69] R.C. Walker et al., Phys. Lett. B234 (1989) 353

Figure captions

Fig.1 Two–pion cut contribution to the isovector nucleon form factors.

Fig.2 Spectral distribution of the isovector form factors weighted with $1/t^2$. Shown are $2\mathrm{Im}F_1^v(t)/t^2$ (long–dashed line), $2\tau\mathrm{Im}F_2^v(t)/t^2$ (short–dashed line) and $2\mathrm{Im}G_E^v(t)/t^2$ (solid line). Upper panel: no ρ–ω mixing. Lower panel: with ρ–ω mixing.

Fig.3 Analytic structure of the fit functions eqs.(36,37) in the complex t plane. (a) Isoscalar case. (1) Poles at M_ω, M_Φ and $M_{S'}$, (2) the singularity at $\Lambda^2 - Q_0^2$ and (3) the right–hand cut starting at Λ^2. The data are given at negative t. (b) Isovector case. The right–hand cut (1) is the two–pion continuum, (2) are the three isovector poles, (3) and (4) are equivalent to (2) and (3) of the isoscalar case.

Fig.4 Optimal fit within the multiplicative parametrization including ρ–ω mixing and the constraint from the neutron charge radius. The data for G_E^n are from [50] [47] [48] [49] [44] [51] [52] [53], for G_E^p from [54] [55] [56] [57] [21] [58] [15] [59] [60] [61], for G_M^p from [54] [55] [57] [21] [58] [59] [68] [69], and for G_M^n from [63] [64] [65] [66] [67]. For the data of ref. [44], we have taken the values based on the Paris potential but enlarged the error bars to account for the model–dependence.

Fig.5 Asymptotic behaviour of the proton magnetic form factor. The best fit in comparison to the available data is shown. Upper panel: $Q^4 G_M^P(Q^2)/\mu_p$, lower panel: $L^{-1}(Q^2) Q^4 G_M^P(Q^2)/(\mu_p L^{-1}(0))$

Fig.6 The ratio $Q^2 F_2^p(Q^2)/F_1^p(Q^2)$ for the best fit compared to the data.

Fig.7 Hadronic (short–dashed lines) versus quark (long–dashed lines) contributions for the isoscalar and isovector Dirac and Pauli form factors (solid lines) in the additive parametrization. The absolute values of the various contributions are shown.

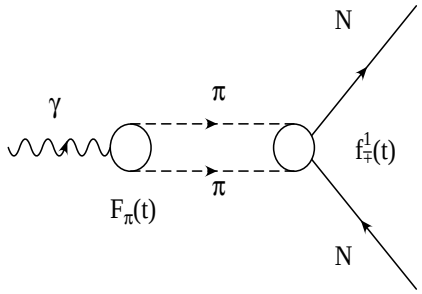

Figure 1

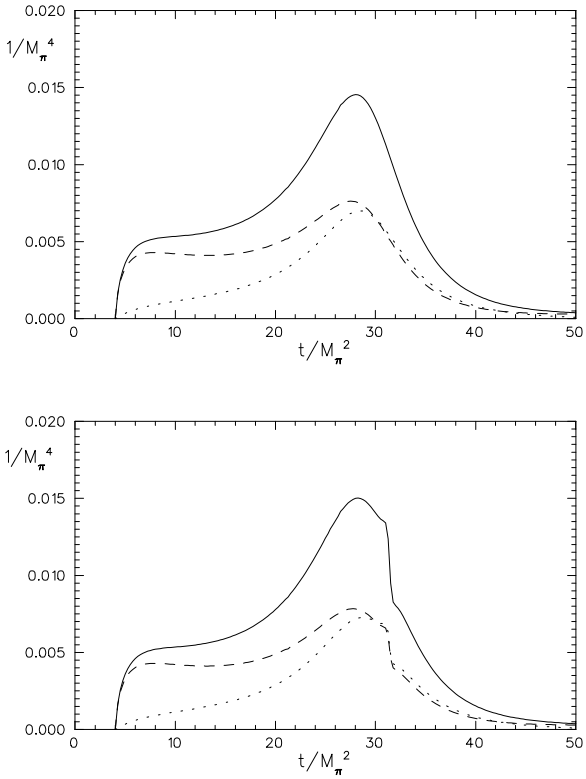

Figure 2

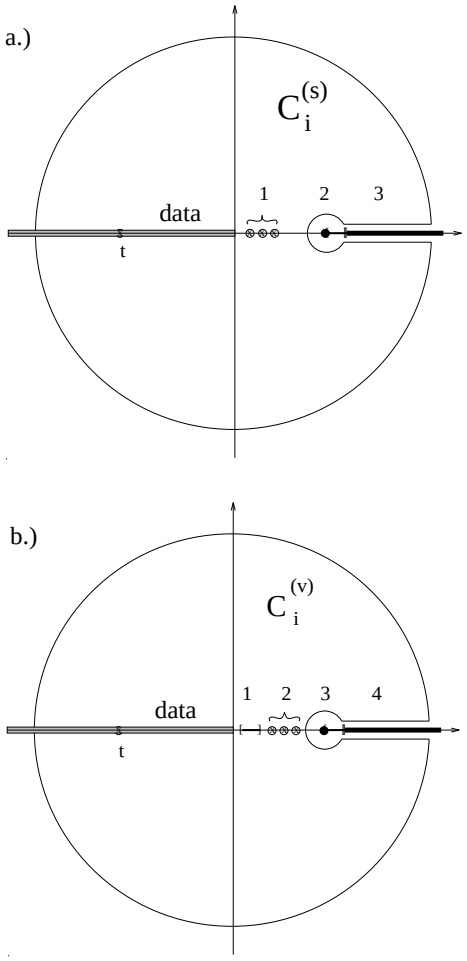

Figure 3

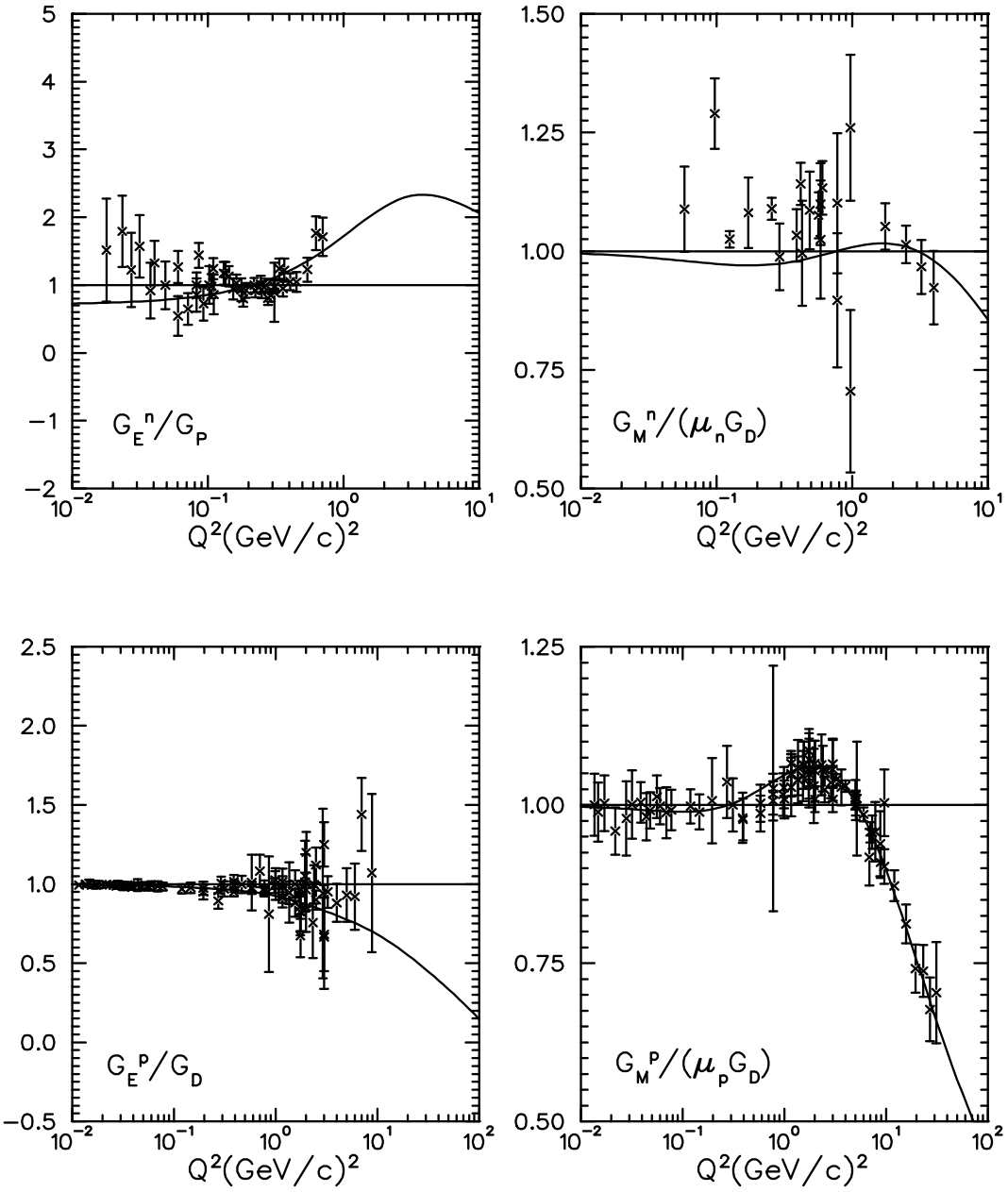

Figure 4

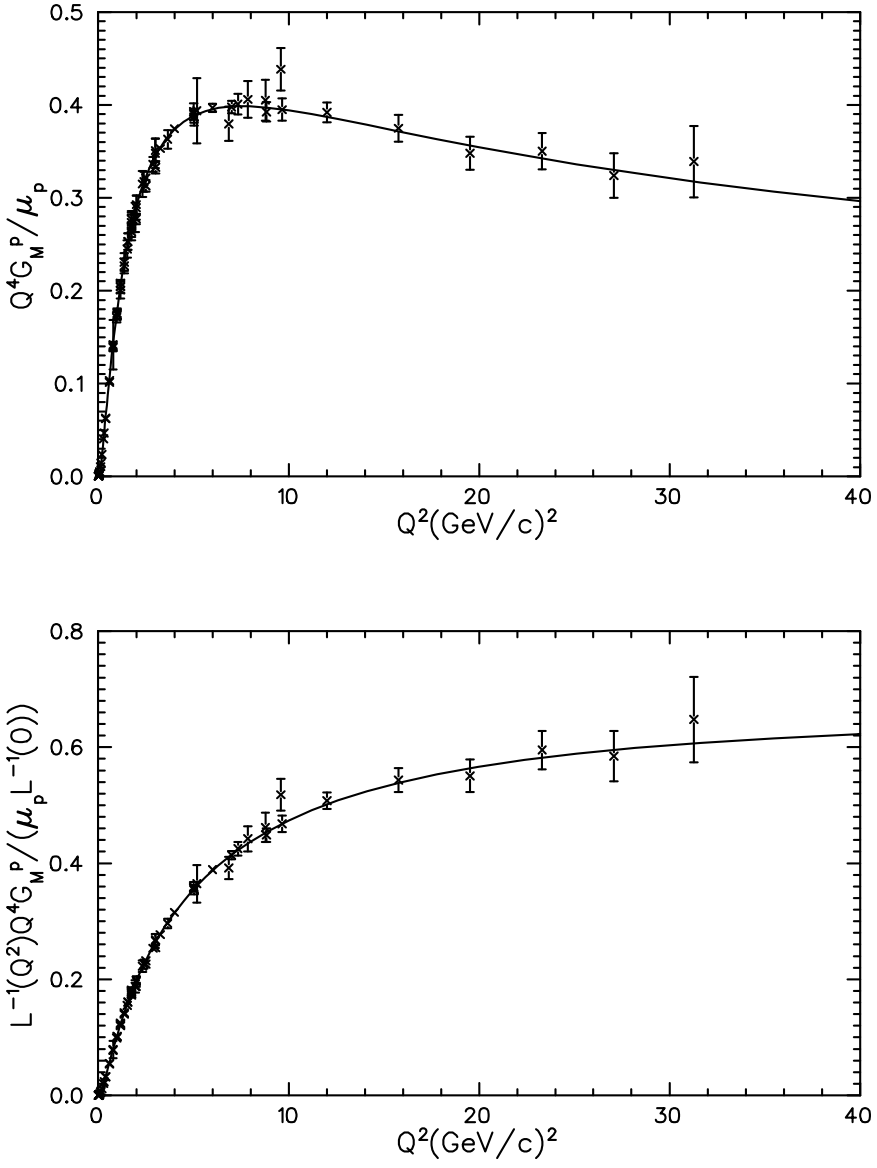
0.5
0.4
0.3
0.2
0.1
0.0
$Q^4G_M^p/\mu_p$
0
10
20
30
40
$Q^2(GeV/c)^2$
0.8
0.6
0.4
0.2
0.0
$L^{-1}(Q^2)Q^4G_M^p/(\mu_p L^{-1}(0))$
0
10
20
30
40
$Q^2(GeV/c)^2$

Figure 5

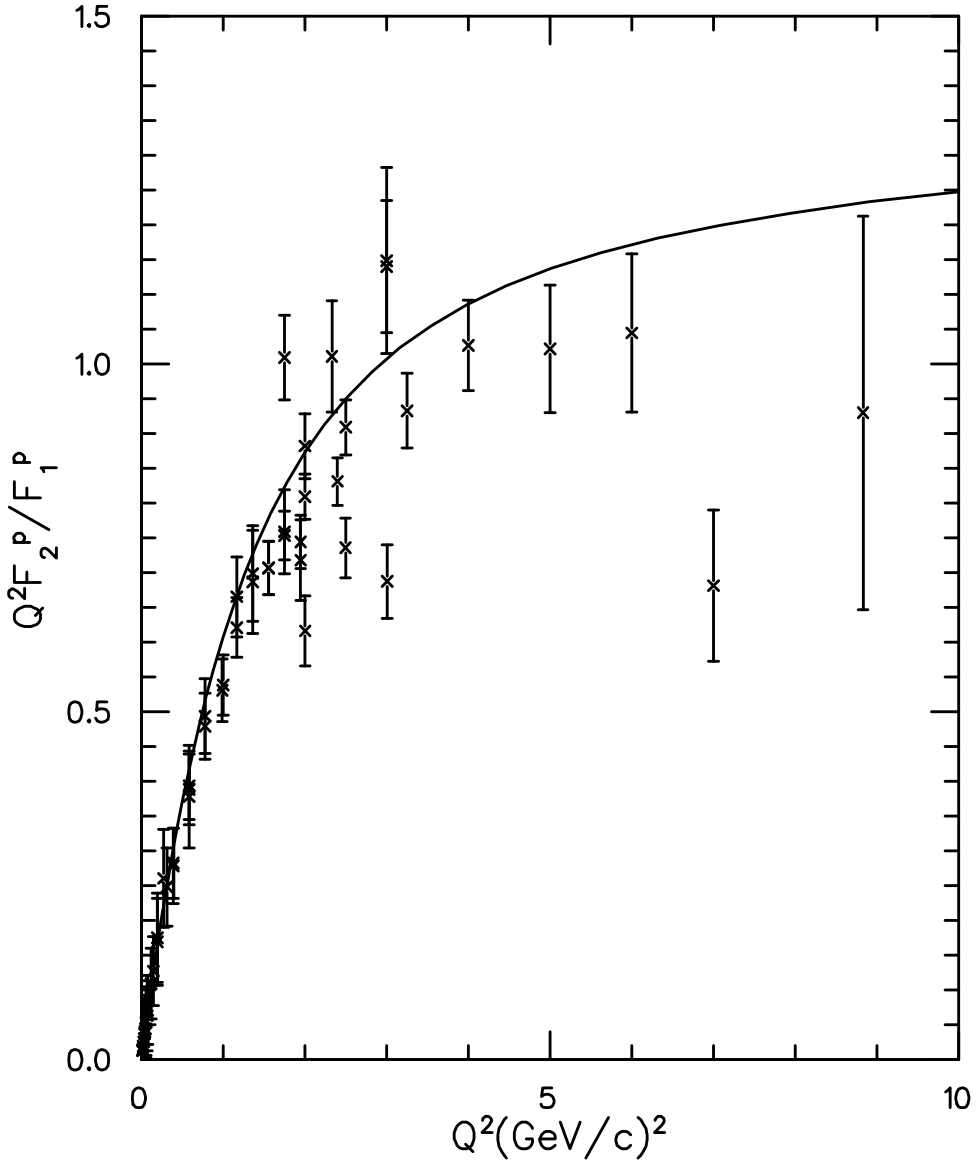

Figure 6

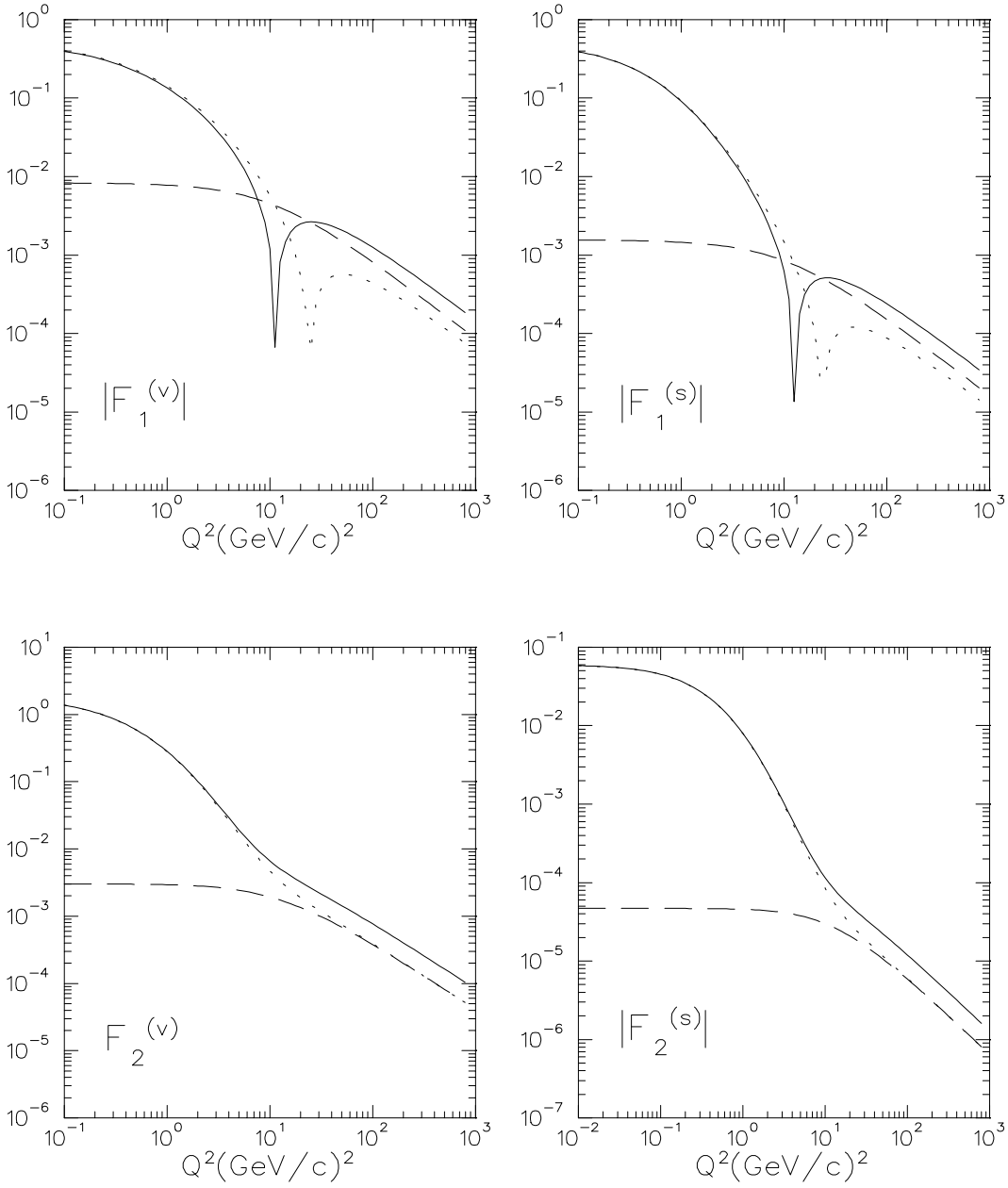

Figure 7